REPORT DOCUMENTATION PAGE

Form Approved
OMB No. 0704-0188

1. REPORT DATE *(DD-MM-YYYY)*	2. REPORT TYPE	3. DATES COVERED *(From - To)*
07/30/2010	Final Report	08/01/2006 to 07/31/2010

4. TITLE AND SUBTITLE
Multi-color long wavelength infrared detectors based on III-V semiconductors

5a. CONTRACT NUMBER

5b. GRANT NUMBER
FA9550-06-1-0457

5c. PROGRAM ELEMENT NUMBER

6. AUTHOR(S)
Omar Manasreh

5d. PROJECT NUMBER

5e. TASK NUMBER

5f. WORK UNIT NUMBER

7. PERFORMING ORGANIZATION NAME(S) AND ADDRESS(ES)
University of Arkansas,
Research Support and Sponsored Program
120 Ozark Hall
Fayetteville, AR 72701. Phone: (479) 575-3845

8. PERFORMING ORGANIZATION REPORT NUMBER
DUNS # 143574726

9. SPONSORING/MONITORING AGENCY NAME(S) AND ADDRESS(ES)
Air Force Office of Scientific Research
875 N. Randolph St. Room # 3112
Arlington, VA 22203

10. SPONSOR/MONITOR'S ACRONYM(S)
AFOSR/PKR3

11. SPONSOR/MONITOR'S REPORT NUMBER(S)
AFRL-OSR-VA-TR-2012-0589

12. DISTRIBUTION/AVAILABILITY STATEMENT
Public domain. No restriction - A

13. SUPPLEMENTARY NOTES

14. ABSTRACT
Several III-V semiconductor material systems were investigated for multi-color photodetectors taking into consideration the enhanced properties of low dimensional systems, such as InAs quantum dots and GaAs quantum rings. The emphasis was placed on detecting both interband and intersubband transitions that form the basis of may optoelectronic devices. The research performed under this grant made it possible to investigate the new nanomaterial systems with properties covering the near infrared and visible spectral ranges. Devices were fabricated and tested. The photoresponse of these multi-color photodetectors was found to cover the mid-infrared spectral ranges as well as the near and visible spectral ranges with dete

15. SUBJECT TERMS
multi-color photodetectors, quantum dots, photoresponce, mid-infrared, near infrared, visible spectral range

16. SECURITY CLASSIFICATION OF:			17. LIMITATION OF ABSTRACT	18. NUMBER OF PAGES	19a. NAME OF RESPONSIBLE PERSON
a. REPORT	b. ABSTRACT	c. THIS PAGE			19b. TELEPHONE NUMBER *(Include area code)*
No restriction	No restriction	No restriction	Unclassified Unlimited		

Multi-color long wavelength infrared detectors based on III-V semiconductors

PI: Omar Manasreh,
Department of Electrical Engineering
3217 Bell Engineering Center
University of Arkansas
Fayetteville, AR 72701
manasreh@uark.edu

AFOSR Grant No. FA9550-06-1-0457

INTRODUCTION

The development of near-infrared (NIR) to far-infrared (FIR) detection is a key technology for many commercial, medical, military, and space applications, e.g., optical communication, smart fire alarms, detection of breast cancer, night vision and missile guidance. In recent years, there has been much interest in using intersubband transitions in quantum dots (QDs) for mid-infrared (MIR) and FIR photodetectors. Quantum dot based devices are expected to have superior optical properties compared to bulk and quantum well structures due to their three-dimensional carrier confinement. One advantage is the ability to absorb normal incident radiation which bypasses the need for corrugations or gratings commonly used in quantum well infrared photodetectors. This advantage eliminates unnecessary processing which in turn decreases the overall fabrication time and complexity. Other potential advantages are higher detectivities to infrared radiation and near room temperature operation which is a direct result of longer carrier capture and relaxation times due to the phonon bottle neck effect. In addition, QDs do not have to be doped in order to observe photoresponse, consequently, reducing the dark current and noise of photodetectors.

Besides great interests in QDs for detector applications, QDs have attracted lots of attentions in photovoltaic applications. QDs have been proposed as an ideal system for the practical implementation of intermediate band (IB) solar cells, where the IB could arise from the energy levels of the electronic states confined within the QDs. Due to the phonon bottleneck effect in QDs, it favors the isolation of the IB from the CB preventing fast recombination of the electrons from the CB to the confined states. By forming intermediate band for the absorption of sub-bandgap photons and hence extending the spectral response to the near-infrared region, IB solar cells have the potential for achieving efficiencies of 63.3% for a single junction cell (an equivalent efficiency to a three-junction tandem solar cell) and has been actively investigated.

This report investigates multicolor photodetectors based on interband and intersubband transitions in InAs and InGaAs QDs as a means for room temperature, multi-color photodetection in the visible to MIR range. Moreover, this report explores the application of QDs in solar cells.

The devices were fabricated using standard processing techniques consisting of photolithography, chemical wet etching, metal deposition, lift-off and rapid thermal annealing. For n-i-n photodetectors, AuGe(88:12)/Ni/Au (75nm/20nm/300nm) are used as metal contacts and for p-i-n solar cells, AuGe(88:12)/Ni/Au and AuZn are used as n-type and p-type contacts, respectively. Material characterization is conducted by using atomic force microscopy, photoluminescence technique, electrochemical capacitance voltage, and Fourier transform

spectroscopy. Device characterization is carried out using many tools, such as Keithley 4200 Semiconductor Characterization System, a Bruker IFS 125HR FT infrared spectrometer equipped with NIR and MIR sources, a Perkin Elmer Spectrum GX FT infrared spectrometer, AM1.5 standard solar simulator.

DOPING EFFECT ON INTERBAND AND INTERSUBBAND MULTICOLOR INFRARED PHOTODETECTORS:

First, many samples and devices were prepared through the duration of the grant. As an example, four samples A, B, C, and D based on InAs QDs will be discussed in this section. The samples are grown by molecular beam epitaxy on a semi-insulating GaAs substrate. The bottom contact layer consists of a 0.5 μm n-type GaAs:Si layer with [Si] = 1 x 10^{18} cm^{-3}. Following the bottom contact layer, a spacer layer composed of 50 nm of GaAs was grown at 580°C. InAs (2 ML) QDs are grown at 500°C using the Stranski-Krastanov (S-K) growth mode. A 50 nm GaAs cap layer was grown after the growth of the QDs. The QD layer is repeated 10 times and the QD region is doped to different levels (for samples A, B, C, and D, undoped, 1×10^{17}, 5×10^{17}, and 1×10^{18} cm^{-3}, respectively). Finally, a 0.3 μm n-type GaAs:Si [Si] = 2×10^{18} cm^{-3} top contact layer is grown.

The photoresponse spectra for all samples measured at 77 K are shown in Fig. 1 (left). Two bands are observed covering NIR (0.83 μm – 1.0 μm) and MIR (5 μm – 8 μm) at 77 K. The NIR band spectra are measured at 1.0 V for samples A and B, at 0. 9 V for sample C and 0.2 V for sample D. MIR band spectra are obtained at 77 K under different bias voltages for maximum photoresponse. The confined energy levels in conduction and valence band at 300 K are calculated using Comsol Multiphysics® 3.4 based on step potential barrier and effective mass approximations. The calculated energy levels are shown in Fig. 1 (right). The NIR features are attributed to interband transitions from the confined hole states, labeled HH and LH for heavy hole and light hole, to confined electron states, labeled E. From calculation, the interband transitions correspond to LH3→E3 and LH4→E4. The extension to longer wavelength is due to transitions from deeply confined states, from which electrons have small tunneling probability to contribute to photoresponse. Furthermore, the electron ground-state energy level E_1 is calculated to be about 184 meV above InAs conduction band while the electron first excited state E_2 is about 380 meV from the bottom of the potential well. Therefore, the $E_1\rightarrow E_2$ transition (~196 meV or ~6.3 μm) is the main contribution to the MIR response. As the doping level increases in the QDs, significant change is observed for both NIR and MIR spectra. The maximum photoresponse in the near infrared region is observed from the undoped InAs quantum dot infrared photodetector, whereas the maximum photoresponse in the middle infrared region is observed from the quantum dot infrared photodetector with Si doped to 1×10^{17} cm-3. With further increase doping concentration, the NIR band rapidly disappears and MIR also show observable decrease. These observations suggest that trade-off in doping density need to be made to achieve optimum detection at both bands and high doping concentration leads to poor detector performance due to increased dark current and dopant introduced defects.

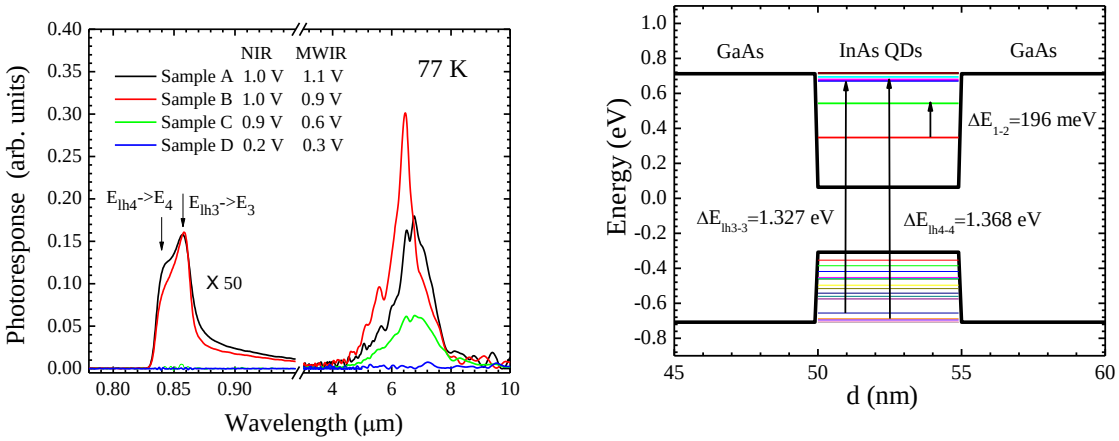

Figure 1. *(Left) Dual band photoresponse spectra of samples A, B, C, and D. MWIR band is the maximum photoresponse intensity at different bias voltages at 77 K. (Right) The calculated energy levels in InAs quantum dots using step potential barrier and effective-mass*

HIGH TEMPERATURE DOT-WELL INTERBAND AND INTERSUBBAND DUAL-BROADBAND PHOTODETECTORS:

Quantum-dots-in-a-well (DWELL) structures have been investigated as a promising candidate for high performance MIR and LWIR detection, due to lower dark current, good control over the operating wavelength, and enhanced quantum confined Stark effect (QCSE). In this sectio, we investigated different DWELL structures for high temperature infrared photodetectors. Three InAs/InGaAs/GaAs DWELL samples, E, F, and G, are grown on semi-insulating GaAs substrates by the MBE technique. General QDIP structure is adopted. For sample E, two monolayers of undoped self-assembled S-K InAs quantum dots are capped with with a 10 nm $In_{0.15}Ga_{0.85}As$ QW and 50nm GaAs spacer, which are also repeated 10 times. Samples F and G have similar structures, which consist of 2 monolayers of self-assembled S-K InAs QDs grown at 500°C and 5.7 nm graded $In_xGa_{1-x}As$ (x=0.15 to 0 for sample F and x=0.3 to 0 for sample G) quantum well as the cap layer. The purpose of the graded cap layer is to create multiple quantized energy levels on the InGaAs graded barrier to achieve broadband detection.

The photoluminescence spectra for the DWELL samples at 77 K are displayed in Fig. 2. The energy transitions in the InAs QDs of samples E, F, and G are measured to be 1.18 eV, 1.07 eV, and 1.09 eV, respectively. The transition from the QDs in a graded well (sample F and G) is significantly broader than QDs in a traditional well (sample E). Therefore, QDs in a graded well are promising for broadband detection. The dark current in a photodetector is the current that originates from sources other than excitation. There are three major components in the dark current: 1.) sequential resonant tunneling; 2.) thermionic emission; and 3.) field-assisted tunneling. The dark current for samples E, F, and G measured from 77 to 300 K is shown in Fig. 3. The asymmetric band structure of the samples produces an asymmetric dark current in the negative and positive range. The two main factors governing the increase in dark current are voltage and temperature. The dark current will increase with an increase of temperature due to the thermionic emission of the carriers. The dark current in sample E is higher than those of sample F and G, which is due to the band structure of each of the structures. For sample G, the

dark current at 1 V was 4.3 x 10^{-9} and 4.8 x 10^{-4} A at 77 and 300 K, respectively. Although, the room temperature dark current is significantly higher than the dark current at 77 K, it is considerably lower than most quantum well detectors. In order to further reduce the dark current, $Al_{0.3}Ga_{0.7}As$ current blocking layers can be added.

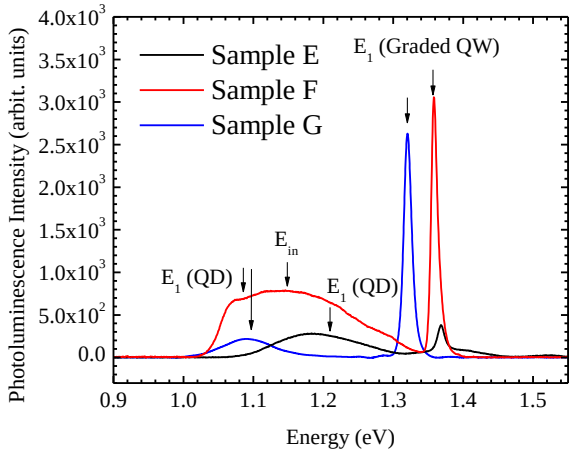

Figure 2. *Photoluminescence of samples E, F, and G measured at 77 K.*

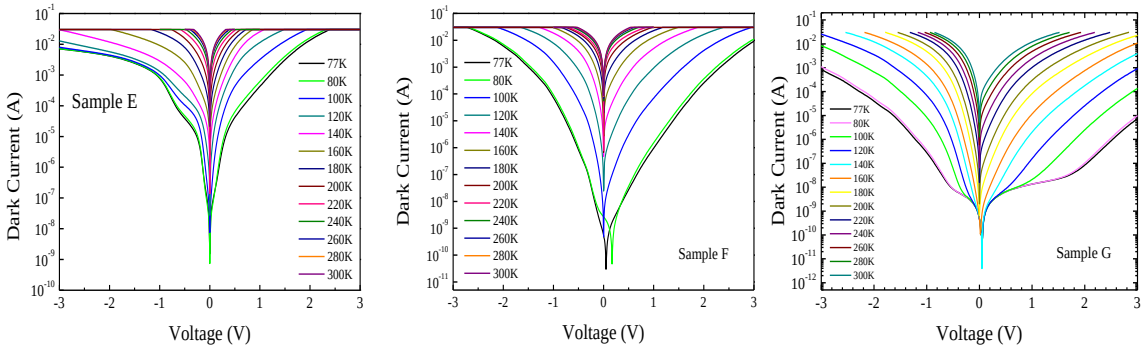

Figure 3. *The dark current from 77 to 300 K for an (left) sample E, (middle) sample F (right)* sample G.

The dual broadband photoresponse spectra at 300 K for sample E, F, and G are shown in Fig. 4. NIR and MIR dual-broadband photoresponse are observed from both sample F and sample G while only NIR photoresponse is observed from sample E. The absence of MIR photoresponse of sample E may be due to the high dark current. Due to the graded well, sample F shows two broad photoresponse bands. As the grading change to 45%, the photoresponse

linewidth increase even more. The MIR photoresponse of sample G is measured as a function of

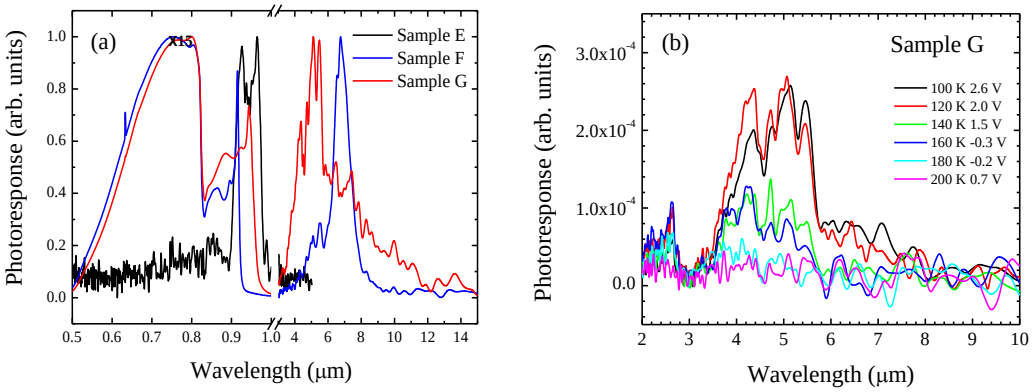

Figure 4. *(a) The dual broadband photoresponse at room temperature for sample E, F, and G in the visible to the MIR region. The MIR photoresponse is not observed for sample E. (b)*

temperature, as shown in Fig. 4 (b). The photoresponse remains observable up to 160 K. Such high temperature operation is mainly due to the low dark current and makes such detectors promising for electrical-cooled detection systems.

VOLTAGE-TUNABLE MULTICOLAR QUANTUM DOT INFRARED PHOTODETECTOR WITH CASCADE BARRIERS

In order to further decrease dark current as well as tune the operating wavelength by voltage, we propose a novel QDIP incorporated with additional cascade barriers. Besides the typical QDs used in active region, cascade barrier is incorporated in each layer. Fig. 5 displays the schematic of the device structure of one period as well as the calculated energy levels. The asymmetric dark current-voltage characteristics are shown in Fig. 6 (a). At positive bias voltages, the energy levels in the CBs become more squeezed, which narrowed the path for electrons without affecting the photocurrent as the continuum align with the energy band in the CBs. Low dark current has been observed at positive bias voltages as expected. However, at negative bias voltages, the energy levels in the CBs spread out which largely increases the dark current. In Fig. 6 (b) are presented three-color photoresponse spectra. At MIR range, the photoresponse peak can be voltage-tuned from ~4 μm to ~8 μm, which most likely from E1 to continuum and E2 to E4 transitions, respectively. At negative bias voltages, the high density injection makes the lower energy states, such as E1, overwhelmed with electrons. For this reason, the photoresponse peak shifts to longer wavelength and can only be observed at a low bias voltage. On the other band, the position of visible-NIR band is not affected by applied voltage because the transitions are most from near and above GaAs band edges.

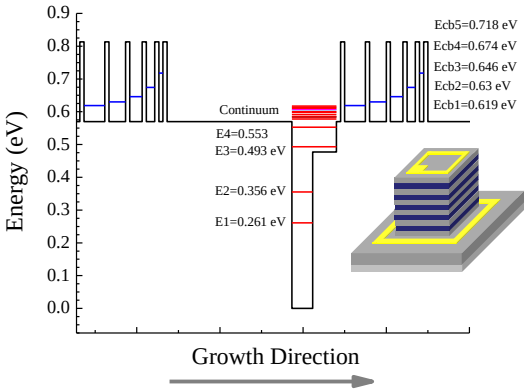

Figure 5. *The conduction band structure and calculated energy levels of the DWELL. The Insert is a schematic of a fabricated device.*

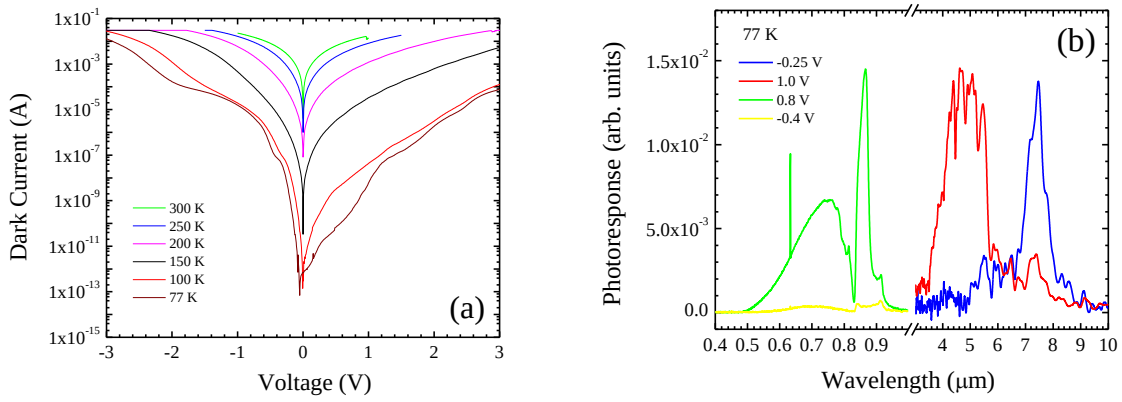

Figure 6. *(a) Dark current of the DWELL photodetector at different temperatures. (b) Visible-NIR and MIR dual band photoresponse spectra at various voltages.*

EFFECTS OF PROTON IRRIDIATION ON QDIPS WITH DIFFERENT FLENCES

Despite the advantages discussed above, recent study showed that the QD structures and QD-based devices are much more resistant to irradiation than bulk semiconductors or quantum wells. Robust materials that can be resistant to the impact of radiation-induced degradation in optoelectronic devices are therefore very important for space application and extensive research have been done to determine the survivability of the optoelectronic devices in harsh proton irradiated environment

In this report, Effect of 2 MeV proton irradiation on InAs quantum dot photodetectors is investigated using fluences in the range of 9.0×10^{10} – 5.0×10^{14} cm^{-2}, as shown in Fig. 7. The

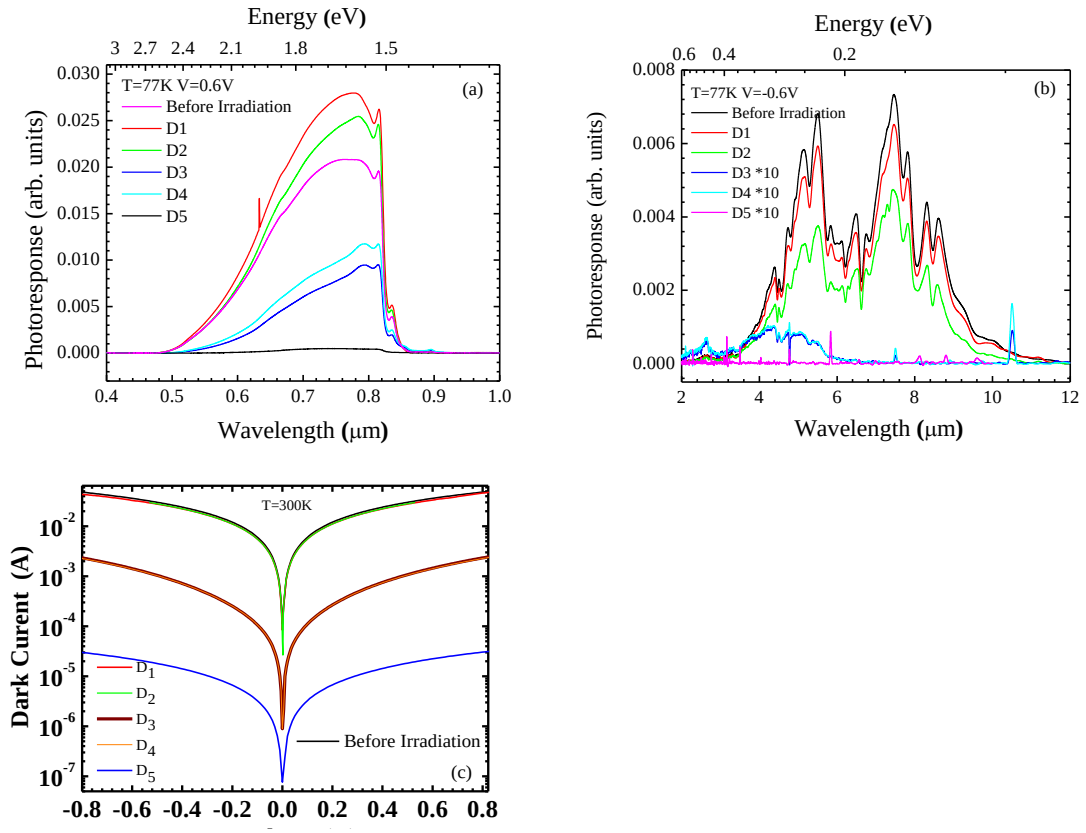

Figure 7. *(a) NIR photoresponse spectra under different Proton irradiation fluences. (b) MIR photoresponse spectra under different Proton irradiation fluences. (c) I-V characteristics under different Proton irradiation flences.*

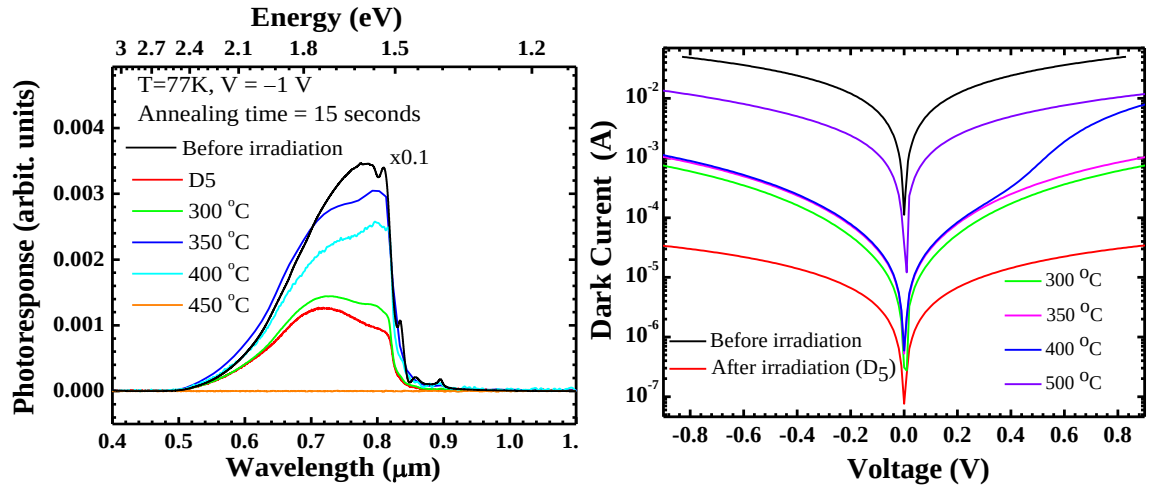

Figure 8. *(a) NIR photoresponse measured after different annealing temperatures. (b) Dark current of the detector after different annealing temperatures.*

intensity of the photoresponse spectra are found to slightly increase when the devices are irradiated with low level fluencies and then decrease by about two orders of magnitude when the

devices are irradiated with a fluence of 5.0×10^{14} cm^{-2}. The dark current as a function of the bias voltage is measured before and after irradiation. These results are interpreted in terms of proton irradiation induced atomic displacement defects.

Rapid thermal annealing is performed for the heavily irradiated devices and a partial recovery of the photoresponse is observed, as shown in Fig. 8 (a). The rapid thermal annealing is performed for 15 seconds at 300, 350, 400, and 450 °C. The photoresponse spectrum of the device before irradiation is plotted after scaling it by a factor of 0.1. There is an initial recovery of the photoresponse when the device is annealed at 300 and 350 °C. The intensity of the spectrum is decreased after annealing the device at 400 °C then the photoresponse is completely depleted after annealing the device at 450 °C.

The partial thermal annealing recovery of the photoresponse may be due to the annealing of defects and traps, such as interstitials and vacancies. The defects can trap dimensional electron gas, but once these defects are annealed out, the electrons are released leading to the observed recovery. This conclusion is supported by the current voltage (I-V) characteristics shown in Fig. 8 (b) where the dark current increases as the annealing temperature is increased. The complete depletion of the photoresponse after the device is annealed at 450 °C is most likely to be due to the failure of the metallic contacts.

STRAIN-FREE MULTICOLOR PHOTODETECTORS

The self-assembled lattice mismatched In(Ga)As/GaAs systems have been used as the active region for quantum dots infrared photodetectors as discussed in previous discussions. However, lattice-matched nanostructure systems, such as GaAs/AlGaAs, have not been developed for device application, which is mainly due to the incompatibility of Stranski–Krastanow growth mode with the latticematched systems. In this report, we present multicolor photodetectors fabricated from strain-free GaAs nanostructures embeded in lattice-matched $Al_{0.3}Ga_{0.7}As$ matrix using droplet epitaxy technique. By using droplet epitaxy technique, various

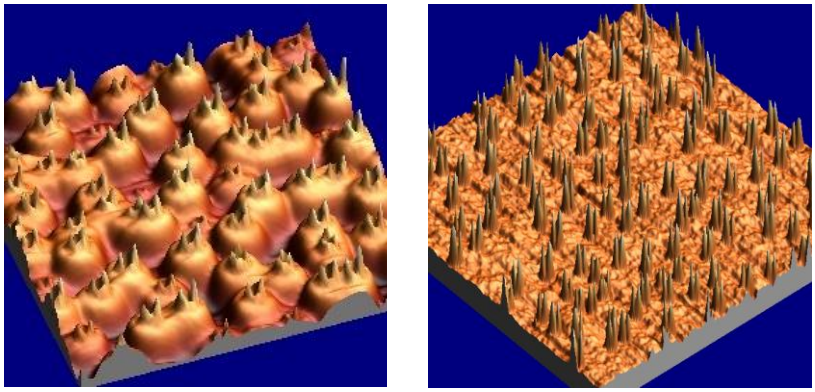

Figure 9. *(Left) GaAs quantum rings by low temperature droplet epitaxy. (Right) GaAs quantum dot pairs grown on AlGaAs by high temperature droplet epitaxy.*

nanostructures can be grown from lattice-matched structures as shown in Fig. 9. A GaAs/ $Al_{0.3}Ga_{0.7}As$ photodetector shows a multicolor visible-NIR and MIR photoresponse in Fig. 10. The mid infrared photoresponse band is observed in the spectral region of 2.0 – 6.0 μm as shown in Fig. 10 (a). The spectra were measured at 77 K for different bias voltages. This band is attributed to the intersubband transitions within the conduction band of GaAs/ $Al_{0.3}Ga_{0.7}As$

multiple quantum rings. The several peaks in the spectra are most likely due to the variation of the quantum ring height and shape. The device photoresponse in the visible-near-infrared spectral region was measured from 77 K to room temperature for different bias voltages of 1.5 V, as shown in Fig. 10 (b). The spectra show two broad-bands resulting from the quantized levels in the GaAs quantum rings as well as $Al_{0.3}Ga_{0.7}As$ barriers. The broadband response at visible-NIR region could make this structure very useful for photovoltaic applications. The detectivity, D*, is estimated to be on the order of 5.2×10^{9} cm•Hz^{½}W at 0.83 μm at room temperature and 2.0×10^{10} cm•Hz^{½}W 5.10 μm for the interband and intersubband transitions, respectively. In addition, the detector has also been found work the photovoltaic mode from 77 K to 300 K.

To increase the material quality of nanostructures from droplet epitaxy, high temperature droplet epitaxy is used to grow GaAs quantum dots. As the growth temperature increases, the diffusion rate of Ga increase, which makes the quantum rings evolve into quantum dot pairs. Also, the crystallization rate becomes faster leading to better crystal for device applications. The GaAs quantum dot pairs were grown in $Al_{0.3}Ga_{0.7}As$ matrix and repeated for ten times. Same as the quantum ring photodetector, the measured photoresponse spectra also cover almost the entire spectra and the transitions from the quantum confined states in quantum dots are clearly illustrated in Fig. 11. Also shown in Fig. 11 are the PL and IV curves of the quantum dot pairs detector. The dominate PL peak at ~1.77 eV is a strong evidence of quantum confinement and the broadband PL spectrum is due to size variation of the dot pairs. In addition to the photoresponse due to the interband transitions in the visible-near-infrared spectral region, another broadband photoresponse band was observed in the mid infrared spectral range of 2.0 – 8.0 μm as shown in Fig. 11 (b). The spectra were measured at 80 K for bias voltages of 0.4 V and 1.3 V. This mid infrared band is as a result of the intersubband transitions within the conduction band of $GaAs/Al_{0.3}Ga_{0.7}As$ coupled QDs. With increasing bias voltage, the photoresponse intensity increases because of field-assisted tunneling of photo-excited electrons. Besides photodetector applications, the GaAs/AlGaAs nanostructures demonstrate great potentials for photovoltaic applications. The premise is supported by the facts that no strain is involved in the system, and such nanostructures could solve the reduced Voc and Isc problem in current InAs quantum dots based intermediate band solar cells.

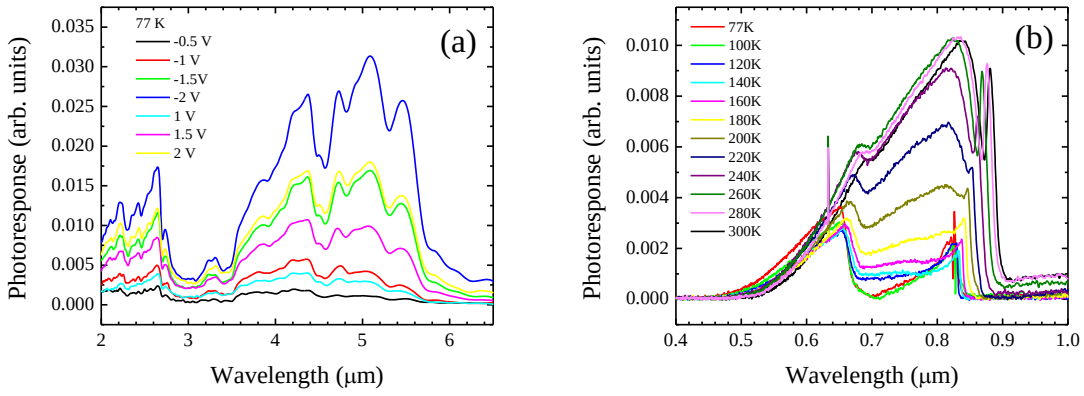

Figure 10. *(a) Photoresponse in the MIR band at 77 K (b) Visible-NIR hotoresponse spectra at different temperatures for a bias voltage of 1.5 V.*

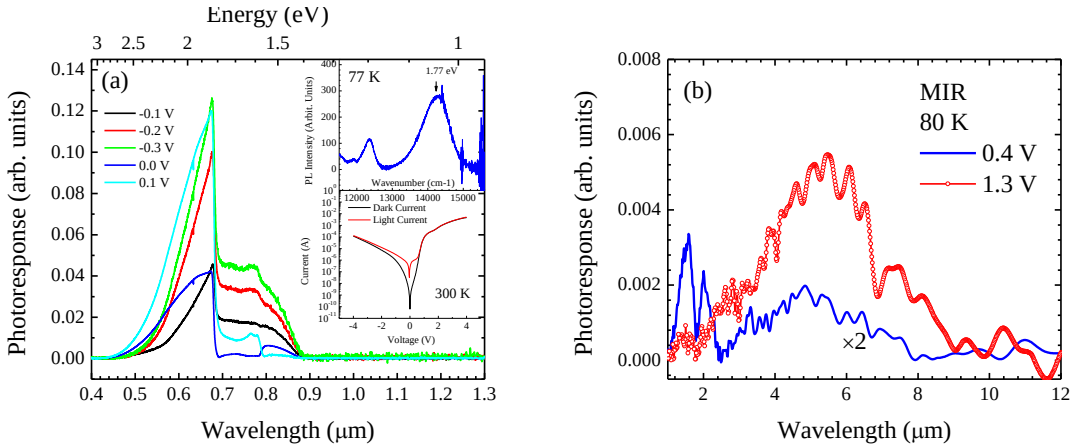

Figure 11. *(a) Photoresponse in the MIR band at 77 K (b) Visible-NIR hotoresponse spectra at different temperatures for a bias voltage of 1.5 V.*

ANNEALING EFFECTS ON QUANTUM DOT SOLAR CELLS

So far, quantum dots (QDs) are one of the most promising candidates to realize the intermediate band in solar cells. These QDs based solar cells have received a considerable research interest in the last few years because of their potential for high solar energy conversion efficient using only a single junction. The QDs based photovoltaic devices are flexible in terms of band gap engineering to meet specific needs. This flexibility provides a mean to tune the energy levels leading to an enhancement of optical properties and the performance of the device. Rapid thermal annealing has been used as a method to fine adjust the energy levels and enhance the structural and optical quality of nanostructures.

The photoresponse spectra of all annealed solar cells compared with the unannealed reference solar cell are shown in Fig. 12. All the QD solar cells have demonstrated response to long wavelength illumination beyond the GaAs band edge of 870 nm. This confirms that all cells under annealing treatment are contributing to the extra short-circuit current by introducing an intermediate band comparing to a single junction GaAs solar cell without InAs QDs. As shown in Fig. 12, the photoresponse spectra at long wavelength region (>900 nm) have a large blueshift as annealing temperatures increase. The IV characteristics of the QD solar cells under different post annealing conditions are shown in Fig. 13. The short circuit current and cell efficiency decreases at annealing temperatures up to 700 °C. With annealing temperature increased beyond 700 °C, both short circuit current and efficiency increase. Since the photoresponse almost remains the same at low annealing temperatures, the reduction in short circuit current and efficiency may not be attributed to the changing position of intermediate band. Such decrease in short circuit current may be explained by increased recombination sites created by inhomogeneous In-Ga diffusion during low temperature annealing. Although the changing position of the intermediate band in the cell is due to low EIC transition rate for InAs/GaAs QD cells, rapid thermal annealing still holds the promise of tuning the intermediate band to obtain the optimum band configuration. Moreover, high temperature annealing at 800 ºC has increased the cell short circuit current density from 12.6 mA/cm^2 to 13.3 mA/cm^2 and lead to 5.4% increase in efficiency as a result of improved structure quality.

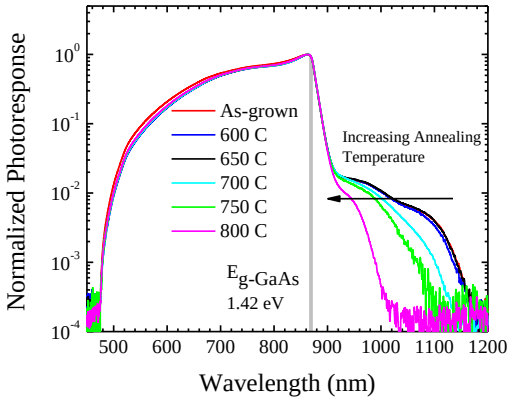

Figure 12. *Normalized photoresponse spectra of InAs QD solar cells with different annealing temperatures at 300 K.*

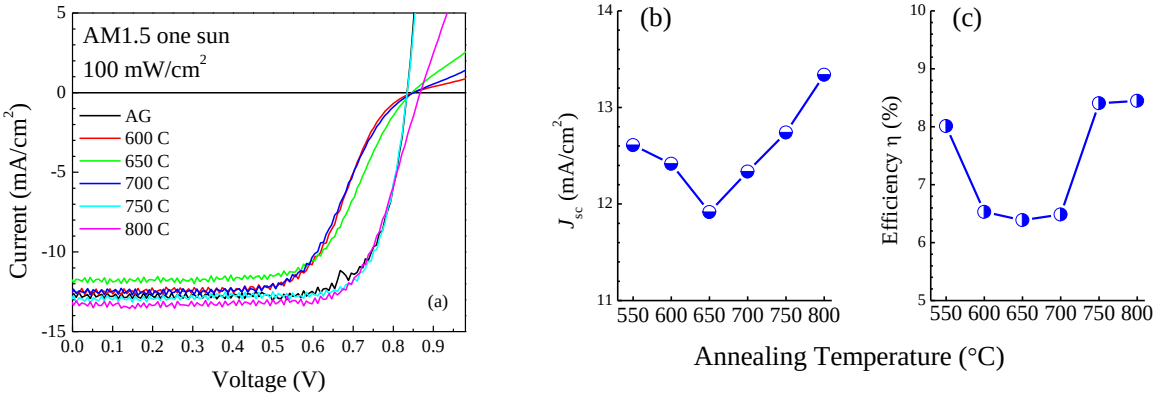

Figure 13. *(a) I–V characteristics of InAs QD solar cells under AM 1.5 one Sun illumination and dark environment. Measured short circuit current density Jsc (b) and efficiency η (c) of solar cells with different annealing conditions.*

List of technical papers supported by the AFOSR grant:

1. "*InGaAs Quantum Well Grown on High Index Surfaces for Superluminescent Diode Applications*" Zhenhua Li, Jiang Wu, Zhiming M. Wang, Dongsheng Fan, Aqiang Guo, Shibing Li, Shui-Qing Yu, Omar Manasreh, and Gregory J. Salamo, Nanoscale Research Letters 5, 1079-2084 (2010).
2. "*Influence of template type and buffer strain on structural properties of GaN multilayer quantum wells grown by PAMBE*," V. P. Kladko, A. V. Kuchuk, N. V. Safryuk, P. M. Lytvyn, V. G. Raicheva, V. F. Machulin, A. E. Belyaev, Yu. I. Mazur, E. A. DeCuir Jr, M. E. Ware, M. O. Manasreh, and G. J. Salamo, Appl. Phys. Lett. (submitted).
3. "*Intersubband Infrared Photodetector with Strain-Free GaAs Quantum Dot Pairs Grown by High Temperature Droplet Epitaxy*," Jiang Wu, Dali Shao, Vitaliy G. Dorogan, Alvason Z. Li, Shibin Li, Eric A. DeCuir, Jr., M. Omar Manasreh, Zhiming M. Wang, Yuriy I. Mazur, and Gregory J. Salamo Nano Letters **10**, 1512-1516, (2010).
4. "*Quantum Ring Infrared Photodetector Based On Droplet Epitaxy Technique*," Dali Shao, Jiang Wu, Zhenhua Li, Omar Manasreh, Vasyl P. Kunets, Zhiming Wang, Gregory Salamo, Material Research Society, Boston, MA Nov 26 – Dec 02, 2009. (accepted).
5. "*Photodetectors fabricated from strain-free GaAs coupled quantum dots*," Jiang Wu, Dali Shao, Zhenhua Li, Omar Manasreh, Vasyl P. Kunets, Zhiming Wang, Gregory Salamo, Material Research Society, Boston, MA Nov 26 – Dec 02, 2009.
6. "*Inter- and intrasubband spectroscopy of cubic AlN/GaN superlattices grown by molecular beam epitaxy on 3C-SiC*," C. Mietze, E.A. DeCuir, Jr., M.O. Manasreh, K. Lischka, and D. J. As, Phys. Stat. Solid. C **7**, No. 1, 64–67 (2010).
7. "*Intermediate-band based on GaAs quantum rings for solar cells*," Jiang Wu, Dali Shao, Zhenhua Li, M. O. Manasreh, V. P. Kunets, Z. M. Wang, and G. J. Salamo, Appl. Phys. Lett. **95**, 071908 (2009).
8. "*Spectroscopy of shallow InAs/InP quantum wire nanostructures*," Yu. I. Mazur, V.G. Dorogan, O. Bierwagen, G. G. Tarasov, E. A. DeCuir, S. Noda, Z. Ya. Zhuchenko, M. O. Manasreh, W. T. Masselink, G. J. Salamo, Nanotechnology **20** 065401 (2009).
9. "*Multicolor photodetector based on GaAs quantum rings grown by droplet epitaxy*," Jiang Wu, Zhenhua Li, Dali Shao, M. O. Manasreh, V. P. Kunets, Z. M. Wang, G. J. Salamo, and B. D. Weaver, Appl. Phys. Lett. **94** 171102 (2009).
10. "*Quantum Ring Infrared Photodetector by Droplet Epitaxy*," Jiang Wu, Zhenhua Li, Dali Shao, Omar Manasreh, Zhiming Wang, and Gregory Salamo, Accepted at Nanotech conference and Expo 2009, Nanoelectronics and Photonics section, Houston, Texas. May 3-7, 2009.
11. "*Cubic GaN/AlN multiple quantum well photodetector*," E. A. DeCuir, Jr., M. O. Manasreh, E. Tschumak, J. Schörmann, D. J. As, and K. Lischka, Appl. Phys. Lett. **92**, 201910-3 pages (2008).

12. "*Growth of nonpolar cubic GaN/AlN multiple quantum wells with intersubband transitions for 1.5 μm applications*," D. J. As, J. Schömann, E. Tschumak, K. Lischka, E. A. DeCuir, and M. O. Manasreh, Phys. Stat. Sol. (c) **5**, 2092-2095 (2008).

13. "*Polarized Raman spectroscopy and X-ray diffuse scattering in InGaAs/GaAs(100) quantum-dot chains*," V. V. Strelchuk, Yu. I. Mazur, Zh. M. Wang, M. Schmidbauer, O. F. Kolomys, M. Ya. Valakh, M. O. Manasreh, G. J. Salamo, J. Mater Sci: Mater Electron **19**, 692 (2008).

14. "*Optical absorption of proton irradiated colloidal CdSe/ZnS core/shell nanocrystals*," K. Y. Narsingi, M. O. Manasreh, and B. D. Weaver, J. Appl. Phys. IEEE Trans. Nuc. Sci. (accepted)

15. "*Room Temperature Near-Infrared Photoresponse Based on Interband Transitions in $In_{0.35}Ga_{0.65}As$ Multiple Quantum Dot Photodetector*," B. S. Passmore, Jiang Wu, M. O. Manasreh, V. P. Kunets, P. M. Lytvyn, and G. J. Salamo, IEEE Electron Device Letters **29,** 224-227 (2008).

16. "*Enhanced photoluminescence from InAs/GaAs surface quantum dots by using a Si-doped interlayer*," B. L. Liang, Yu I. Mazur, Vasyl P. Kunets, Zhiming Wang, G. J. Salamo, E.A. DeCuir, Jr., B. Passmore and M. O. Manasreh Nanotechnology **19**, 065705 (5 pages) (2008).

17. "*Exciton band edges and optical anisotropy of InAs/InP quantum dot structures*", Yu. I. Mazur, S. Noda, G. G. Tarasov, V. G. Dorogan, G. J. Salamo, O. Bierwagen, W. T. Masselink, E. A. DeCuir, Jr., and M. O. Manasreh, J. Appl. Phys. **103**, 054315-7 pages (2008).

18. "*Broadband photoresponse from InAs quantum dots embedded in a graded well for visible to mid-infrared detection*," Brandon S. Passmore, Jiang Wu, Eric A. DeCuir, Jr., Omar Manasreh, P. M. Lytvyn, Euclydes Marega, Jr., Vasyl P. Kunets, and Gregory J. Salamo. Proc. SPIE, Vol. **6900**, DOI:10.1117/12.762338 (2008).

19. "*A voltage-tunable two-color InGaAs/AlGaAs quantum well infrared photodetector*," Brandon Passmore, Jie Liang, Da Zhuang, Omar Manasreh, Vasyl Kunets, Greg Salamo, Mater. Res. Soc. Symp. Proc. **959** M17-14 (2007).

20. "*1.37 - 2.90 Micron Intersubband Transitions in GaN/AlN Superlattices*," Eric Anthony DeCuir, Jr., Emil Fred, Omar Manasreh, Jinqiao Xie, Hadis Morkoc, Esther Baumann, Daniel Hofstetter, Mater. Res. Soc. Symp. Proc. **955** I13-01 (2007).

21. "*Dual broad-band photodetector based on interband and intersubband transitions in InAs quantum dots embedded in graded InGaAs quantum wells*," B. S. Passmore, Jiang Wu, M. O. Manasreh, and G. J. Salamo, Appl. Phys. Lett. **91**, 233508-3 (2007).

22. "*Multi-color Photoresponse Based on Interband and Intersubband Transitions in InAs and InGaAs Quantum Dot Photodetectors*," B. S. Passmore, J. Wu, E. A. Decuir, Jr., M. O. Manasreh, P. M. Lytvyn, E. Marega, Jr., Vas. P. Kunets, G. J. Salamo, Materials Research Society Fall Meeting, Boston, MA (2007).

23. "*Near Infrared Intersubband Detectors fabricated from Cubic and Hexaonal GaN/AlN Superlattices*," E. A. DeCuir, Jr, E. Fred, M. O. Manasreh, J. Schörmann, D. J. As, K.

Lischka, M. Wares, and G. Salamo, Materials Research Society Fall Meeting, Boston, MA (2007).

24. "*Proton Irradiation Effect on CdSe-ZnS Core-Shell Nanocrystals Embedded in Ultra Violet Curable Resin*", K. Y. Narsingi, M. O. Manasreh, and B. D. Weaver. IEEE Region 5 Technical Conference, Fayetteville, Arkansas, April 20-21, 2007.

25. "*Intersubband Transitions in Quantum Wells Infrared Photodetector*"; Jiang Wu, Brandon Passmore, and M. O. Manasreh, IEEE Region 5 Technical Conference, Fayetteville, Arkansas, April 20-21, 2007.

26. "*Near-infrared Intersubband Absorption in Non-polar Cubic GaN/AlN Superlattices*", E. A. DeCuir Jr, E. Fred, M. O. Manasreh, J. Schörmann, D.J. As, and K. Lischka, Appl. Phys. Lett. **91**, 041911 (2007).

27. "*Photoluminescence properties of InAs/GaAs heterostructure with surface quantum dots sitting on multiple-layer buried quantum dots*." Baolai Liang, Zhiming Wang, Yuriy I. Mazur, Eric A DeCuir, Jr., Omar Manasreh, and Gregory J. Salamo, Materials Research Society, 2006 Fall Meeting.